Mekanika: Majalah Ilmiah Mekanika

Analysis of Stern Flap Application on Planing Hulls to Reduce Resistance Using CFD

Indra Nurul Hidayat[1], Aldias Bahatmaka[1*], Fedrik Immanuel Rumapea[1], Dandi Exada[2]

1 Department of Mechanical Engineering, Universitas Negeri Semarang, Semarang, Indonesia

2 Department of Mechanical Engineering, Universitas Sebelas Maret, Surakarta, Indonesia

* Corresponding Author's email address: aldiasbahatmaka@mail.unnes.ac.id

Keywords:
Planing Hull
Stern Flap
Resistance
CFD
VOF

Abstract
Planing hulls exhibit complex hydrodynamic characteristics at high speeds due to two-phase flow interactions, variations in wetted surface area, and nonlinear pressure distributions, making resistance prediction challenging. This study evaluates the effect of stern flap angle and span width on the total resistance of a planing hull under calm-water conditions. Numerical simulations were conducted using a Reynolds-Averaged Navier–Stokes (RANS)-based Computational Fluid Dynamics approach with a k–ε turbulence model and the Volume of Fluid (VOF) method in ANSYS Fluent. The numerical model was validated against a benchmark CFD study previously verified with Fridsma's experimental data, showing deviations below 5% across the investigated Froude number range. Parametric simulations were performed for stern flap angles of 2°, 4°, and 6° with span widths of 43%, 48%, and 53% of the hull breadth. The results indicate that stern flap configuration significantly affects resistance, particularly under full planing conditions. The optimal configuration was obtained at a span of 53% of the hull breadth with a 2° flap angle, reducing the non-dimensional resistance (R/Δ) from 0.186 to 0.1699 (9.69%) at Fr = 1.8. Trim analysis shows an average reduction of 1.16°, contributing to the observed decrease in resistance.

1 Introduction

Planing hulls exhibit complex hydrodynamic characteristics, especially at high speeds. Under these conditions, the interaction between water and air flow, changes in wet surface area, and non-linear pressure distribution make calculating ship resistance more complicated than for displacement hulls [1]. On the other hand, operational cost constraints and energy efficiency demands drive the need to improve resistance performance in planing hulls [2]. This complexity makes planing hulls an interesting topic in ship architecture, particularly in hydrodynamic analysis and hull shape optimization [3]. Various studies have been conducted to develop energy-saving devices to reduce ship resistance. Several approaches studied include the microbubble injection method, stern wedges, tunnel stern, stern flap, and stepped hull [4,5]. Among these methods, the stern flap shows significant potential due to its ability to modify the flow under the transom and increase lift [6].

https://dx.doi.org/10.20961/mekanika.v25i1.114603

Revised 26 May 2026; received in revised version 08 April 2026; Accepted 28 April 2026
Available Online 30 April 2026

2579-3144

Several studies show that applying stern flaps to planing hulls can reduce total resistance by up to 7% [7]. Planing hulls themselves are considered suitable for the application of stern flaps due to the flow characteristics and pressure distribution on the bottom of the hull, especially at small angles between the hull surface and the water surface [8]. A ship is categorized as a planing hull when it operates at a relatively high Froude Number (Fr), generally Fr ≥ 1–1.2 [1]. One of the experimental studies that is widely used as a reference in Planing hull studies was conducted using the Fridsma Model, which uses simple hull geometry to study hydrodynamic characteristics in planing conditions [9]. The Fridsma model has been widely used by various researchers as a reference case in numerical simulation validation [10]. Several follow-up studies have also been conducted to examine the effect of mesh density and geometric modifications on the accuracy of numerical results, including the application of spray strips, which have been reported to reduce spray wash deflection and lower total resistance [11].

Advances in computing technology have encouraged the increased use of numerical analysis in studies of ship hydrodynamics. However, numerical simulations of planing hulls are still considered less accurate than those of displacement ships due to the complexity of free-surface flows and strong turbulence. Several numerical methods have been used in fluid flow analysis, such as the Finite Element Method, Finite Difference Method, and Finite Volume Method [12]. Among these methods, the Finite Volume Method is most widely applied in fluid dynamics simulations due to its stability and ability to handle turbulent flows [13]. In this context, the Reynolds-Averaged Navier–Stokes (RANS) approach with the k–ε turbulence model and the Volume of Fluid (VOF) method are widely used to model the two-phase flow of water and air around planing hulls [14,15].

Based on this background, this study focuses on a numerical investigation of the effect of stern flaps on the total resistance of planing hulls. The simulation was performed using ANSYS Fluent software with a RANS-based CFD approach and the Volume of Fluid method. This study focuses on evaluating total resistance as the primary hydrodynamic performance parameter under prescribed attitude conditions, without performing fully coupled dynamic motion simulations. Variations in stern flap angle and span width were applied within realistic ranges to observe their effects on resistance changes. The results of this study are expected to provide a clearer picture of the tendency of hydrodynamic performance changes due to the installation of stern flaps. In addition, this study is expected to be a reference for ship designers in their efforts to reduce drag and improve fuel efficiency, which ultimately contributes to reducing energy consumption and emissions from the maritime sector [16,17].

2 Model and Boundary Methods

2.1 Model of the Fridsma hull

This study uses experimental data on the Fridsma hull form as a benchmark and applies *stern flaps*. The experimental data used in this study are shown in Table 1 and Figure 1.

Table 1. Fridsma hull form main dimension [9]

Parameter	Unit	Value
L/B	-	5
L	m	1.143
B	m	0.229
TAF	m	0.081
LCG from AP	m	0.457
VCG from keel	m	0.067
τo	Degree	1.569
β	Degree	20
Δ	kg	10.890
Iyy = Izz	kg.m2	0.235

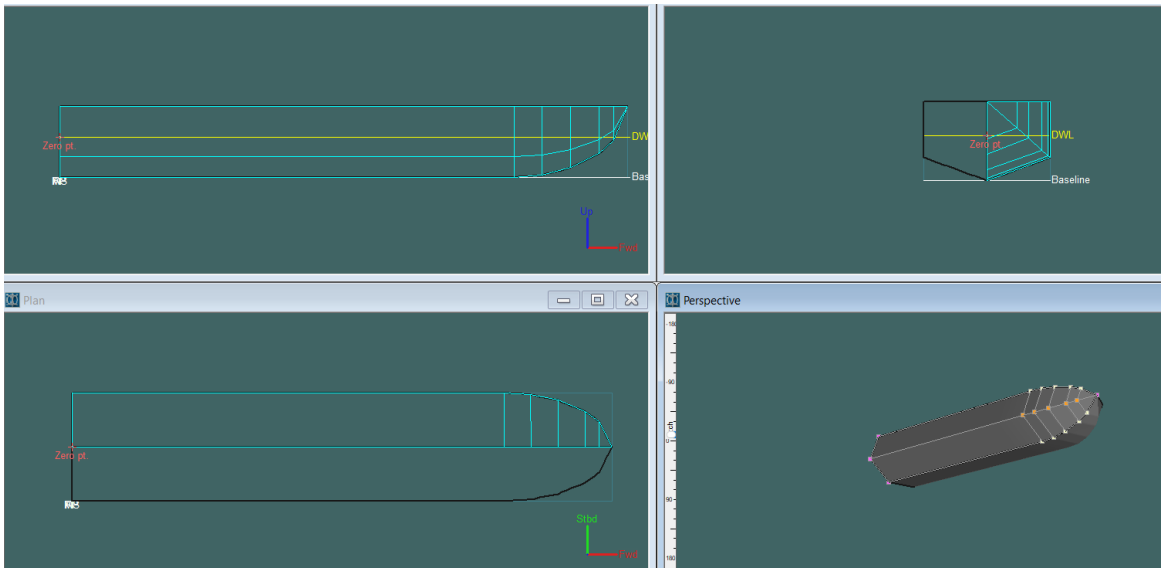

Figure 1. Fridsma hull form

2.2 Stern flap design

A stern flap is a hydrodynamic device in the form of a flat plate applied to the rear of the ship (stern) at a certain angle of inclination to the hull bottom. This device modifies the flow under the stern by increasing local pressure and hydrodynamic lift, thereby reducing trim and affecting the ship's resistance characteristics [18].

The effect of stern flaps on hydrodynamic performance is highly dependent on the combination of flap angle, size, speed conditions, and hull characteristics. The relationship between flap angle changes, pressure distribution, and two-phase flow interaction makes an experimental approach alone inefficient in terms of cost and time [19,20]. Therefore, Computational Fluid Dynamics (CFD)-based numerical simulations are an important tool for systematically evaluating stern flap performance. Through CFD simulations, pressure distribution, flow changes in the transom area, and total drag change trends can be analyzed in greater detail without the limitations of physical testing [21,22].

This study will analyze the effect of variation in stern flap angle on ship resistance. The Stern Flap configuration visualization is shown in Figure 2.

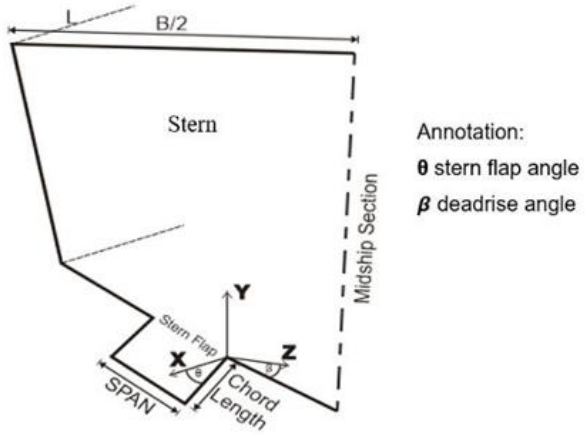

Figure 2. Stern Flap parameter

Span width will be based on the ship's width breadth (B), which is 43%, 48%, and 53% of B, as shown in Figure 3. The stern flap is applied at three different angles: 2°, 4°, and 6°, as shown in Figure 4.

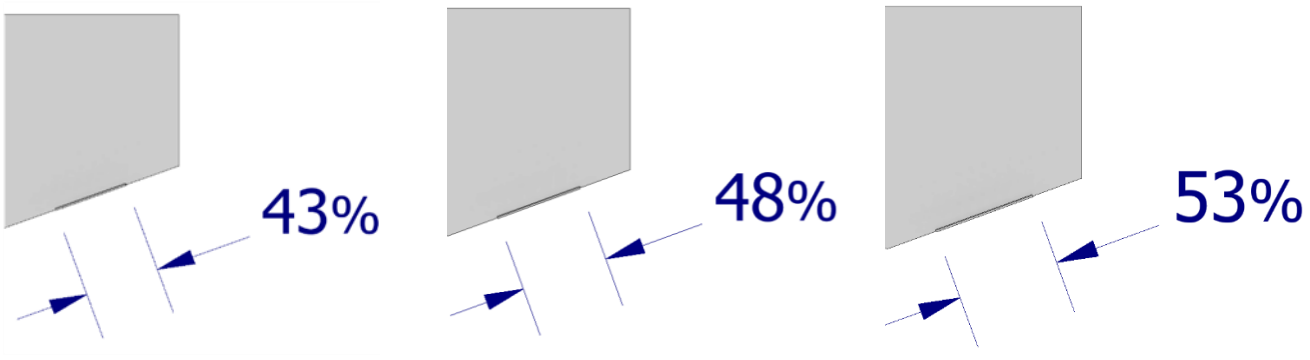

(a) (b) (c)

Figure 3. Configuration of stern flap (a) Span 43%, (b), Span 48%, (c) Span 53%

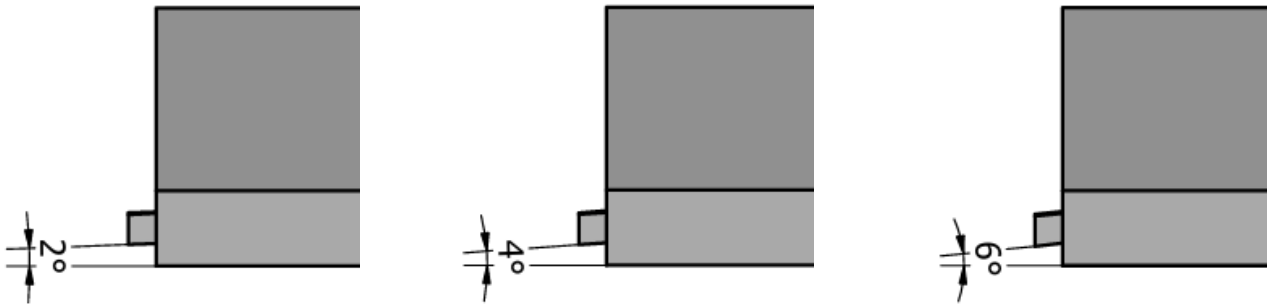

(a) (b) (c)

Figure 4. Configuration of angles stern flap: (a) Stern flap 2°, (b) Stern flap 4°, (b) Stern flap 6°

2.3 Numerical method

The computational domain was constructed to simulate two-phase water-air flow around the planing hull under calm-water conditions. To minimize boundary effects, the inlet boundary was positioned 2.0L upstream of the bow, while the outlet boundary was located 2.5L downstream of the stern. The domain width was set to 1.5L in the transverse direction. Vertically, the domain extended 1.0 L above the free surface and 2.0 L below it to adequately capture wave development and pressure distribution. The computational domain and boundary conditions are illustrated in Figure 5.

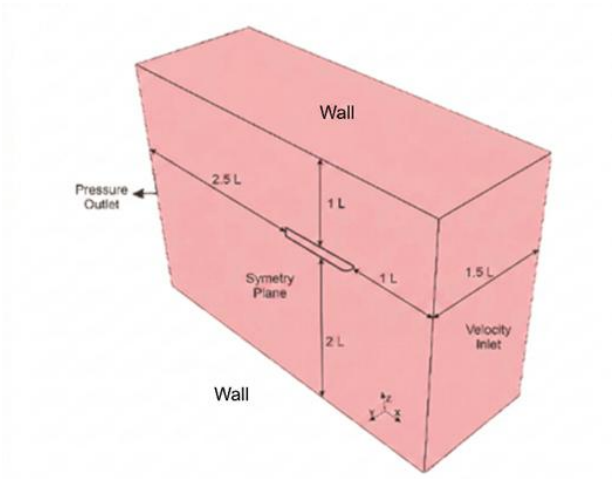

Figure 5. Fluid domain and boundary conditions

The upstream boundary was defined as a velocity inlet with an inflow velocity determined according to the specified Froude number, while the downstream boundary was set as a pressure outlet. A symmetry plane was applied along the longitudinal center plane to reduce computational cost. The top and bottom boundaries of the domain were defined as wall boundaries. The hull surface and stern flap were modeled as no-slip walls [23].

Numerical simulations were performed using ANSYS Fluent software by solving the Reynolds-Averaged Navier-Stokes (RANS) equations for turbulent flow. The Volume of Fluid (VOF) method was applied to model the interaction of two phases, namely water and air, so that the free surface phenomenon could be represented well [24]. The numerical method used was the Finite Volume Method, which is widely used in fluid flow simulations due to its stability and accuracy in handling complex flows [12]. The momentum equation was discretized using a second-order scheme, while the pressure and velocity coupling was solved using the SIMPLE (Semi-implicit Method for Pressure-Linked Equations) algorithm [25]. Gravity was activated to represent the flow's physical conditions realistically.

The simulations were conducted under steady-state conditions to obtain the total resistance of the hull in calm water. In naval architecture, calm-water resistance is defined as the force required to maintain steady motion at a constant speed. Although free-surface flows are inherently unsteady, a steady-state RANS-VOF approach was adopted to obtain mean calm-water resistance values, as commonly applied in planing hull CFD studies [26,27]. The drag force history was monitored throughout the iterations until fluctuations became negligible, and the final resistance value was taken after the integral forces converged.

The VOF model was employed to capture the air–water interface. The volume fraction equation was discretized using a compressive scheme with the Geo-Reconstruct method to maintain a sharp free-surface representation. A second-order upwind scheme was used to discretize the momentum equations spatially. The Courant number was controlled to ensure numerical stability. Local mesh refinement was applied near the free surface and around the hull to improve wave and pressure resolution. The vertical domain extent was selected sufficiently large to minimize artificial wave reflection effects. This VOF configuration follows common practice in free-surface CFD simulations of planing hulls [28].

The turbulence model used in this study is the k–ε model, which has been widely applied in ship hydrodynamic simulations due to its stability and relatively low computational requirements [25]. The selection of the k–ε turbulence model is further supported by previous numerical investigations on planing and Fridsma-type hulls, where RANS k–ε simulations demonstrated satisfactory agreement with experimental and benchmark resistance data [29]. These studies indicate that the k–ε model provides acceptable accuracy in predicting calm-water resistance for high-speed planing hulls while maintaining computational robustness and efficiency.

Although more advanced turbulence models, such as SST k–ω, may offer improved predictions of flow separation in highly nonlinear free-surface flows, the standard k–ε model has been shown to yield reliable resistance estimates for Fridsma-type configurations within the investigated Froude-number range. Therefore, it is considered appropriate for the present parametric investigation.

The k–ε turbulence model consists of two transport equations: the turbulent kinetic energy, denoted by k, and the turbulent dissipation rate, denoted by ε. Turbulent kinetic energy has been modeled as Equation (1).

$$\frac{\partial}{\partial t}(\rho k) + \frac{\partial}{\partial x_i}(\rho k u_i) = \frac{\partial}{\partial x_j}\left[\left(\mu + \frac{\mu_t}{\sigma_k}\right)\frac{\partial k}{\partial x_j}\right] + G_k + G_b - \rho\varepsilon - Y_M + S_k \quad (1)$$

Meanwhile, turbulent dissipation is modeled as Equation (2).

$$\frac{\partial}{\partial t}(\rho\varepsilon) + \frac{\partial}{\partial x_i}(\rho\varepsilon u_i) = \frac{\partial}{\partial x_j}\left[\left(\mu + \frac{\mu_t}{\sigma_\varepsilon}\right)\frac{\partial \varepsilon}{\partial x_j}\right] + C_{1\varepsilon}\frac{\varepsilon}{k}(G_k + C_{3\varepsilon}G_b) - C_{2\varepsilon}\rho\frac{\varepsilon^2}{k}S_\varepsilon \quad (2)$$

where $x_i$represents the spatial coordinates, $\rho$is the fluid density, $E_{ij}$is the mean strain-rate tensor, and $\mu_t$is the turbulent (eddy) viscosity, the turbulent viscosity is modeled as in Equation (3).

$$\mu_t = \rho C_\mu \frac{k^2}{\varepsilon} \quad (3)$$

The implementation of the k–ε model in this study follows the formulation provided in the ANSYS Fluent Theory Guide [30]. The combination of the k–ε model with the Reynolds-Averaged Navier–Stokes (RANS) approach and the Volume of Fluid (VOF) method has been shown to provide adequate accuracy for planing hull simulations [31].

Mesh generation was performed in a three-dimensional computational domain using a polyhedral mesh. Local mesh refinement was applied around the hull and free-surface region to better capture the pressure distribution and viscous effects. The computational mesh configuration is illustrated in Figure 6. The use of polyhedral elements enhances numerical stability and convergence efficiency while maintaining accuracy in complex flow regions [32]. A grid independence study was subsequently conducted using five mesh densities, and the results are summarized in Table 2. The number of elements ranged from approximately 1.12 million to 9.70 million. The results indicate that the variation in total resistance decreases with mesh refinement. The difference in resistance between the fourth mesh (6.0 million elements) and the finest mesh (9.70 million elements) was only approximately 0.11%. Therefore, the fourth mesh was selected as it provides a good balance between computational cost and numerical accuracy.

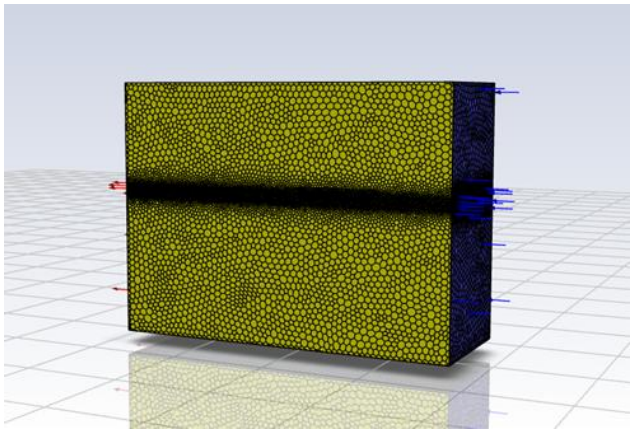

Figure 6. Mesh generation in the current study

Table 2. Grid independence study

Froude Number (Fr)	Element	Resistance (N)	R/Δ	Avg y+	Convergent at Iteration	Error
0.6	1.12 M	14.3602	0.135	495.413	95	
0.6	1.68 M	14.4646	0.136	398.286	104	0.73%
0.6	2.85 M	14.4204	0.136	344.690	131	0.31%
0.6	6.00 M	14.4417	0.136	296.438	177	0.15%
0.6	9.70 M	14.4583	0.136	265.746	156	0.11%

For near-wall treatment, standard wall functions were employed in conjunction with the k–ε turbulence model. For standard and non-equilibrium wall functions, the first near-wall cell should lie within the logarithmic layer region of the boundary layer, typically corresponding to $30 < y^+ < 300$ [33]. The

average y^+ value on the hull surface for the selected mesh was approximately 296. This value remains within the recommended range for the logarithmic layer for standard wall functions.

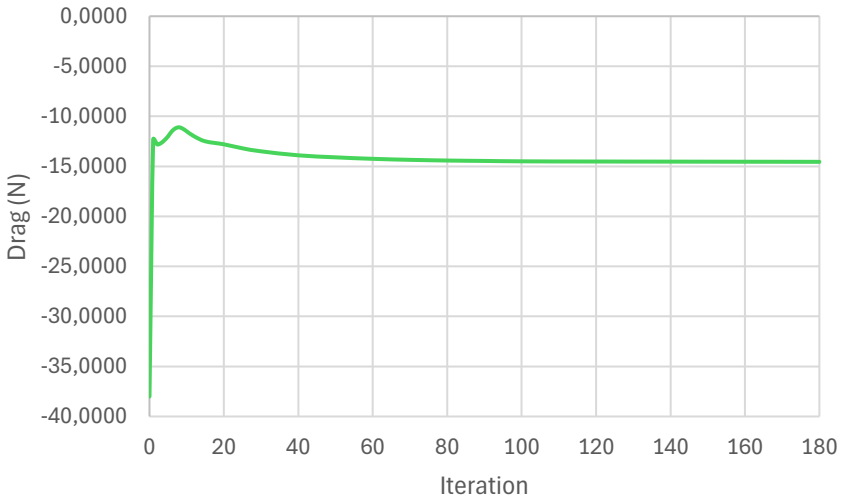

Figure 7. Convergence history graph

The simulation was conducted under steady-state conditions and was run until convergence was achieved. Convergence was indicated by the residuals of the governing equations decreasing below 10^{-5} and the stabilization of the drag force value during the iterative process. The drag force history for the selected mesh is presented in Figure 7. The curve shows initial fluctuations during early iterations, followed by gradual stabilization. After approximately 80 iterations, the drag variation became negligible, indicating that the integral hydrodynamic force had reached a steady value.

The primary parameter analyzed in this study was the total resistance acting on the hull. The total resistance was obtained through the integration of pressure and viscous forces over the hull and stern flap surfaces [34]. The simulation results were subsequently analyzed for each variation in stern flap angle and span width to evaluate their effects on the total planing-hull resistance.

3 Results and Discussion

3.1 Validation

The numerical model in this study was validated by comparing the non-dimensional total resistance (R/Δ) obtained from the present simulation with the benchmark CFD study reported in [7], which was previously validated against Fridsma experimental data. The comparison indicates that the present results follow a trend highly consistent with the benchmark simulation across the entire investigated Froude number range (Fr = 0.6–1.8). As summarized in Table 3, the deviation between the present study and the benchmark data ranges from 0.62% to 1.88%, with an average deviation of approximately 1.03%.

Table 3. Validation results for total resistance

Froude Number (Fr)	Resistance (N) Present Study	R/Δ Present Study	R/Δ Reference [7]	Error Present Study vs Reference
0.6	14.4417	0.136	0.135	0.82%
0.9	15.9141	0.150	0.153	1.88%
1.2	17.4010	0.164	0.165	0.62%

1.5	18.6408	0.176	0.174	0.94%
1.8	19.7590	0.186	0.188	0.88%

In numerical hydrodynamics studies, a validation error below 5% is generally considered acceptable and indicates good agreement between numerical predictions and benchmark data [28]. The benchmark study used for comparison was previously validated against Fridsma's experimental measurements [7]. The close agreement observed in the present study, therefore, indicates that the developed numerical model can reproduce experimentally validated hydrodynamic trends with acceptable engineering accuracy. Minor discrepancies observed at higher Froude numbers are consistent with the inherent challenges of modeling highly nonlinear free-surface planing flows. Consequently, the present validation may be regarded as an indirect validation against experimental data through a benchmark numerical model that has already demonstrated experimental consistency.

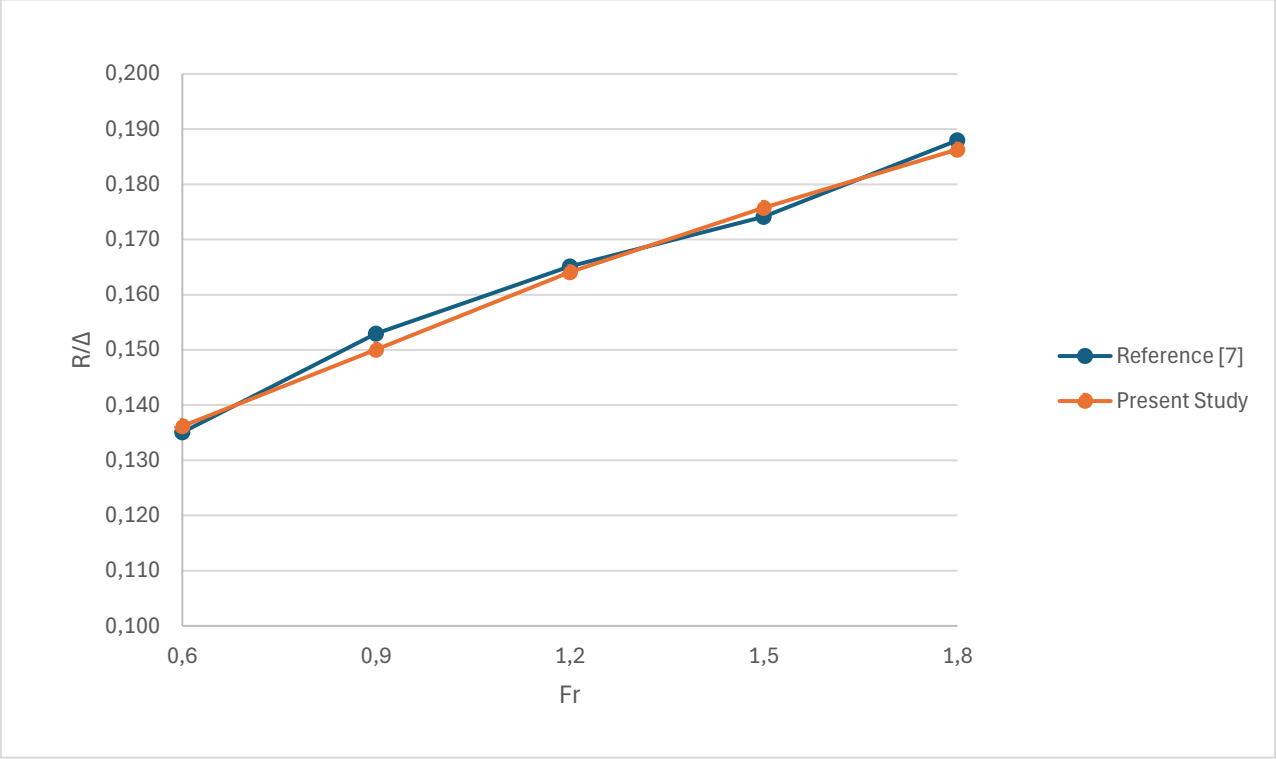

Figure 8. Validation results for total resistance

Figure 8 shows that both the reference and present simulations exhibit a similar upward trend in total resistance as the Froude number increases, particularly from the transition regime to full-planing conditions. Although minor discrepancies between numerical predictions and experimental measurements persist, especially at higher Froude numbers, such differences are common in planing-hull simulations due to complex free-surface and spray phenomena. Therefore, the numerical model is considered sufficiently validated and suitable for subsequent parametric analysis.

3.2 Results

The present study evaluates the combined effect of stern flap angle (2°, 4°, and 6°) and span width (43%, 48%, and 53% of the hull breadth, B) on the non-dimensional total resistance (R/Δ) of the planing hull at various Froude numbers. Figure 9 compares total resistance across all stern flap configurations and the bare hull condition.

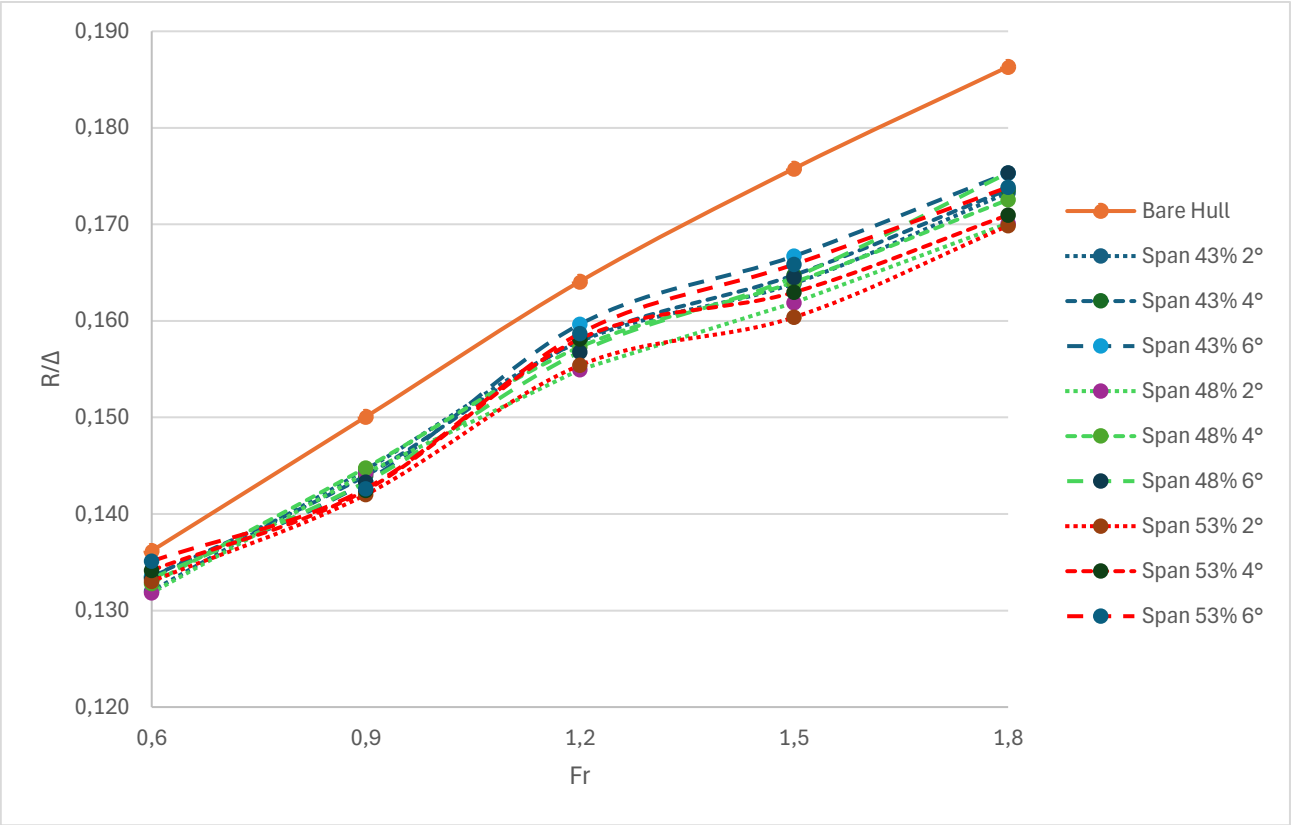

Figure 9. Total resistance comparison

As shown in Figure 9, all stern flap configurations reduce total resistance compared to the bare hull across the investigated Froude number range. The reduction becomes more pronounced as the vessel approaches full planing conditions (Fr ≥ 1.5). Among all tested cases, the configuration with 53% span (relative to breadth) and a 2° flap angle consistently produces the lowest total resistance.

Table 4. Summary of the total resistance

Froude Number (Fr)	R/Δ Span 43%			R/Δ Span 48%			R/Δ Span 53%		
	2°	4°	6°	2°	4°	6°	2°	4°	6°
0.6	0.1320	0.1335	0.1335	0.1318	0.1328	0.1333	0.1330	0.1342	0.1351
0.9	0.1446	0.1440	0.1434	0.1443	0.1448	0.1433	0.1420	0.1425	0.1426
1.2	0.1579	0.1579	0.1597	0.1550	0.1573	0.1568	0.1554	0.1582	0.1587
1.5	0.1639	0.1647	0.1667	0.1619	0.1640	0.1645	0.1604	0.1630	0.1659
1.8	0.1733	0.1736	0.1753	0.1701	0.1725	0.1753	0.1699	0.1710	0.1739

Table 4 presents the comparison of non-dimensional total resistance (R/Δ) for all stern flap configurations at different Froude numbers. The results show that the configuration with a span of 53% of the hull breadth and a 2° flap angle consistently produces the lowest resistance among the tested cases, particularly at higher Froude numbers. At Fr = 1.8, the bare hull exhibits R/Δ = 0.186, whereas the 53%–2° configuration reduces it to approximately 0.1699. Similarly, at Fr = 1.5, the resistance decreases from about 0.176 for the bare hull to 0.1604 for the same configuration. These results indicate that the application of a stern flap with a moderate angle and wider span effectively improves the hydrodynamic performance of the planing hull within the investigated parameter range.

Table 5. Resistance reduction of optimal stern flap configuration

Froude Number (Fr)	Bare Hull	Span 53% 2°	Reduction
0.6	0.1362	0.1330	2.37%
0.9	0.1501	0.1420	5.67%
1.2	0.1641	0.1554	5.58%
1.5	0.1758	0.1604	9.60%
1.8	0.1863	0.1699	9.69%

To quantify the performance improvement of the optimal configuration, the percentage reduction in total resistance relative to the bare hull was calculated and is summarized in Table 5. The results indicate that the reduction in resistance increases with increasing Froude number. At low speed (Fr = 0.6), the reduction is relatively small at approximately 2.37%. However, as the vessel approaches full planing conditions, the reduction becomes more significant. At Fr = 1.5 and Fr = 1.8, the resistance reduction reaches approximately 9.60% and 9.69%, respectively. This trend indicates that the stern flap becomes more effective at higher speeds, where hydrodynamic lift plays a dominant role in reducing trim and pressure resistance. Increasing the flap angle to 4° and 6° generally results in higher resistance, particularly at high Froude numbers. Although a larger angle increases stern lift, it also intensifies the adverse pressure gradient near the transom, potentially promoting flow separation and increasing pressure drag. This observation is consistent with previous findings that suggest the optimal stern flap angle lies within a relatively small range and depends strongly on operating speed and hull characteristics [28,30]. When considering the span effect, increasing the span width from 43% to 53% of the hull breadth generally enhances the reduction in resistance at higher speeds. A wider span enlarges the effective lifting area beneath the stern, enabling improved pressure redistribution without requiring a large flap angle. This confirms that span width plays a critical role in optimizing stern flap performance.

To further investigate the hydrodynamic mechanism associated with the optimum configuration, trim predictions were performed using Maxsurf Resistance based on the Savitsky semi-empirical method. The Savitsky semi-empirical method is widely applied for planing hull performance prediction, as it estimates trim and resistance by solving force and moment equilibrium under planing conditions.

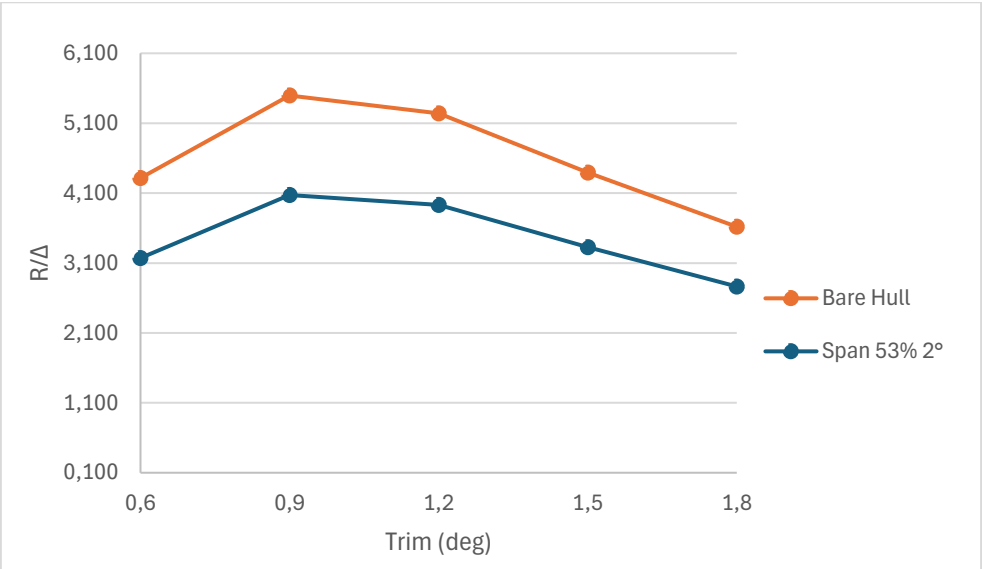

Figure 10. Trim angle comparison

Table 6. Summary of the trim angle variation

Froude Number (Fr)	Bare Hull (deg)	Span 53% 2° (deg)
0.6	4.318	3.170
0.9	5.496	4.072
1.2	5.242	3.929
1.5	4.393	3.326
1.8	3.619	2.764

The trim comparison between the bare hull and the optimal 53%–2° configuration is presented in Figure 10 and Table 6. The results show a consistent reduction in trim angle across all Froude numbers. At Fr = 0.9, trim decreases from 5.50° (bare hull) to 4.07°, representing a reduction of approximately 1.42°. At Fr = 1.5, trim decreases from 4.39° to 3.33°, and at Fr = 1.8 from 3.62° to 2.76°. The average trim reduction across the investigated speeds is approximately 1.16°.

This consistent reduction in trim directly contributes to the observed decrease in resistance. In planing hulls, excessive trim increases wetted surface area and hull angle of attack, leading to higher pressure resistance. By generating additional stern lift, the stern flap modifies the pressure distribution beneath the transom, reduces trim, and consequently lowers total resistance. The consistency between the configuration yielding the lowest resistance and the one producing the lowest trim confirms that resistance reduction is primarily governed by trim modification induced by stern lift. This mechanism aligns with the hydrodynamic behavior described in previous studies [7].

4 Conclusions

This study investigated the influence of stern flap angle and span width on the total resistance of a planing hull using a RANS–VOF-based CFD approach. The results show that both parameters significantly affect hydrodynamic performance, particularly under full planing conditions. The optimal configuration was obtained at a span of 53% of the hull breadth with a 2° flap angle. At Fr = 1.8, the non-dimensional resistance (R/Δ) decreased from 0.186 for the bare hull to 0.1699, corresponding to a reduction of approximately 9.69%. A similar trend was observed at Fr = 1.5, where resistance decreased from 0.176 to 0.1604. Trim analysis using the Savitsky method showed that at Fr = 1.8, the trim angle decreased from 3.62° (bare hull) to 2.76°, while at Fr = 0.9, it decreased from 5.50° to 4.07°, with an average trim reduction of approximately 1.16°. The reduction in trim reduces wetted surface area and pressure resistance. Within the investigated parameter range, a moderate flap angle (2°) combined with a wider span (53% of breadth) provides the most effective configuration for improving the hydrodynamic performance of the planing hull.

5 Acknowledgement

Thanks to the Department of Mechanical Engineering at Universitas Negeri Semarang, especially the Design and Optimization Laboratory, for its support of the research.

References

1. Savitsky Daniel, *Hydrodynamics of High-Speed Marine Vehicles*. New York: Cambridge University Press, 2005.
2. Carlton John, *Marine Propellers and Propulsion*. Burlington: Elsevier, 2007.
3. Y. D. Handiko, A. Bahatmaka, M. Arif Nurul Mustofa, and Y. Dwi Handoko, “Desain dan Analisa Karakteristik Hidrodinamik Pada Lambung Ship-Bus Menggunakan Pemodelan CFD (Computational Fluid Dynamics),” *Enthalpy J. Ilm. Mhs. Tek. Mesin*, vol. 10, no. 2, pp. 98–112, 2025 (*In Indonesian*).
4. A. García-Magariño, S. Sor, R. Bardera, and P. López-Gavilán, “Theoretical model for microbubble drag

reduction technique applied to marine propellers," *Ocean Eng.*, vol. 329, article no. 120797, 2025.
5. R. Niazmand Bilandi, A. Dashtimanesh, S. Mancini, and L. Vitiello, "Comparative study of experimental and CFD results for stepped planing hulls," *Ocean Eng.*, vol. 280, article no. 114887, 2023.
6. J. Zou, S. Lu, Y. Jiang, H. Sun, and Z. Li, "Experimental and numerical research on the influence of stern flap mounting angle on double-stepped planing hull hydrodynamic performance," *J. Mar. Sci. Eng.*, vol. 7, no. 10, article no. 346, 2019.
7. U. Budiarto, S. Samuel, A. A. Wijaya, S. Yulianti, Kiryanto, and M. Iqbal, "Stern Flap Application on Planing Hulls to Improve Resistance," *Int. J. Eng. Trans. C Asp.*, vol. 35, no. 12, pp. 1184-1191, 2022.
8. L. J. Doctors, "Hydrodynamics of transom-stern flaps for planing boats," *Ocean Eng.*, vol. 216, article no. 107858, 2020.
9. Fridsma Gerard, *A Systematic Study of the Rough-Water Performance of Planing Boats*. New Jersey: Naval Ship Research and Development Center, 1969.
10. S. Jin, H. (Heather) Peng, W. Qiu, R. Hunter, and S. Thompson, "Numerical simulation of planing hull motions in calm water and waves with overset grid," *Ocean Eng.*, vol. 287, article no. 115858, 2023.
11. M. Lakatoš, T. Sahk, H. Andreasson, and K. Tabri, "The effect of spray rails, chine strips and V-shaped spray interceptors on the performance of low planing high-speed craft in calm water," *Appl. Ocean Res.*, vol. 122, article no. 103131, 2022.
12. J. H. Ferziger, M. Perić, and R. L. Street, *Computational Methods for Fluid Dynamics*. Stanford: Springer, 2002.
13. F. R. Menter, *Turbulence Modeling for Engineering Flows*. Pennsylvania: ANSYS Inc., 2011.
14. C. W. Hirt and B. D. Nichols, "Volume of Fluid (VOF) Method for the Dynamics of Free Boundaries*," *J. Comput. Phys.*, vol. 39, pp. 201-225, 1981.
15. A. Bahatmaka, D. F. Fitriyana, S. Anis, A. Y. Maulana, M. Tamamadin, S. W. Lee, and J. H. Cho, "Analytical Review of Numerical Analysis in Hydrodynamic Performance of the Ship: Effect to Hull-Form Modifications," *Mek. Maj. Ilm. Mek.*, vol. 23, no. 1, pp. 54-63, 2024.
16. M. A. Lutfi, A. R. Prabowo, E. M. Muslimy, T. Muttaqie, N. Muhayat, H. Diatmaja, Q. T. Do, S. J. Baek, and A. Bahatmaka, "Leisure Boat Concept Design: Study on the Influence of Hull Form and Dimension to Increase Hydrodynamic Performance," *Int. J. Mech. Eng. Robot. Res.*, vol. 13, no. 1, pp. 139-161, 2024.
17. IMO, *Fourth IMO GHG Study 2020 Executive Summary*. London: International Maritime Organization, 2020.
18. S. Jangam, "CFD based prediction on hydrodynamic effects of Interceptor and flap combination on planing hull," *Ocean Eng.*, vol. 264, article no. 112523, 2022.
19. A. A. Ghyferi, A. Bahatmaka, R. F. Naryanto, L. S. Won, and J. H. Cho, "Enhancing Ship Stability: A Comparative Analysis of Single and Double Chine Hull Configurations of Semi-Planning Hull at High Speed," *Mek. Maj. Ilm. Mek.*, vol. 23, no. 2, pp. 156-167, 2024.
20. W. Seok, S. Y. Park, and S. H. Rhee, "Corrigendum to 'An experimental study on the stern bottom pressure distribution of a high-speed planing vessel with and without interceptors' [Int. J. Nav. Archit. Ocean Eng. (2020) 691-698]," *Int. J. Nav. Archit. Ocean Eng.*, vol. 13, pp. 431–432, 2021.
21. T. S. Nainggolan, D. Chrismianto, A. Trimulyono, D. T. Perkapalan, F. Teknik, U. Diponegoro, and K. U. Tembalang, "Prediksi Komponen Hambatan Total Kapal Fridsma Hull Menggunakan Metode Morphing Mesh," *J. Inovtek Polbeng*, vol. 11, no. 2, pp. 92–97, 2021 (*In Indonesian*).
22. Samuel, R. K. Praja, D. Chrismianto, M. L. Hakim, A. Fitriadhy, and A. Bahatmaka, "Advancing Interceptor Design: Analyzing the Impact of Extended Stern Form on Deep-V Planing Hulls," *CFD Lett.*, vol. 16, no. 5, pp. 59-77, 2024.
23. K. I. Matveev, "CFD Simulations of Basic Stepped-Hull Configurations in Planing Regime Using Star-CCM+ Software," *J. Mar. Sci. Eng.*, vol. 13, no. 7, article no. 1217, 2025.
24. M. Mikulec and H. Piehl, "Verification and validation of CFD simulations with full-scale ship speed/power trial data," *Brodogradnja*, vol. 74, no. 1, pp. 41–62, 2023.
25. F. R. Menter, "Two-equation eddy-viscosity turbulence models for engineering applications," *AIAA J.*, vol. 32, no. 8, pp. 1598–1605, 1994.
26. A. Hosseini, S. Tavakoli, A. Dashtimanesh, P. K. Sahoo, and M. Kõrgesaar, "Performance prediction of a hard-chine planing hull by employing different cfd models," *J. Mar. Sci. Eng.*, vol. 9, no. 5, 2021.
27. A. F. Molland, S. R. Turnock, and D. A. Hudson, *Ship Resistance and Propulsion*. New York: Cambridge University Press, 2011.
28. S. Samuel, A. Trimulyono, and A. W. B. Santosa, "Simulasi CFD pada Kapal Planing Hull," *Kapal J. Ilmu Pengetah. dan Teknol. Kelaut.*, vol. 16, no. 3, pp. 123–128, 2019 (*In Indonesian*).
29. S. M. Sajedi and P. Ghadimi, "Experimental and Numerical Investigation of Stepped Planing Hulls in Finding

an Optimized Step Location and Analysis of Its Porpoising Phenomenon," *Math. Probl. Eng.*, vol. 2020, article no. 3580491, 2020.
30. ANSYS, *Standard k-ε Model*. Pennsylvania: ANSYS, Inc., 2024.
31. F. Pacuraru, A. Mandru, and A. Bekhit, "CFD Study on Hydrodynamic Performances of a Planing Hull," *J. Mar. Sci. Eng.*, vol. 10, no. 10, article no. 1523, 2022.
32. C. Branney, *Development of Optimisation Methodologies for the Internal Combustion Engine Airbox Development of Optimisation Methodologies for the Internal Combustion Engine Airbox*. Belfast: Queen's University Belfast, 2008.
33. ANSYS, *ANSYS Fluent User's Guide – Near-Wall Mesh Guidelines*. Pennsylvania: ANSYS, Inc., 2009.
34. Daniel Savitsky, "Hydrodynamic design of planing hulls," *Mar. Technol. SNAME News*, vol. 1, pp. 71-95, 1964.